



UNSUPERVISED UNMIXING AND SEGMENTATION OF HYPER SPECTRAL IMAGES ACCOUNTING FOR SOIL FERTILITY

K LAVANYA*, R JAYA SUBALAKSHMI, T TAMIZHARASI, LYDIA JANE, AND AKILA VICTOR

Abstract. A crucial component of precision agriculture is the capability to assess the fertility of soil by looking at the precise distribution and composition of its different constituents. This study aims to investigate how different machine learning models may be used to assess soil fertility using hyperspectral pictures. The development of images using a random mixing of different soil components is the first phase, and the hyper spectral bands utilized to create the images are not used again during the analysis procedure. The resulting end members are then acquired by applying the NFINDR algorithm to the process of spectral unmixing this image. The comparison between these end members and the band values of the known elements is then quantified, i.e. it is represented as a graph of band values obtained through spectral unmixing. Finally we quantify the similarities between both graphs and proceed towards the classification of the hyper spectral image as fertile or infertile. In order to classify the hyper spectral image as fertile or infertile, we quantify the similarities between the two graphs. Clustering and picture segmentation algorithms have been devised to help with this process, and a comparison is then made to show which techniques are the most effective.

Key words: Hyper spectral imaging, Spectral unmixing, NFINDR Soil fertility, Machine Learning.

AMS subject classifications. 68T05

1. Introduction. Precision Agriculture refers to a farm management concept involving responding, measuring and observing various field features in an attempt to optimize farming techniques.[1] Also known as satellite farming, the goal of precision agriculture is to maximize field productivity while minimizing utilization of resources such as fertilizers. Recently, precision agriculture has better adopted a spot under the limelight with the development of new technologies under the ambit of GPS, GPRS, satellite imaging and machine learning, however there is an inherent gap in its application in the Indian subcontinent for a number of reasons including but not limited to lack of data, motivation to optimize and implement modern farming techniques, and a lack of infrastructure to develop the same on a large scale. Hyper-Spectral Imaging (or HSI) refers to an emerging concept in satellite imaging focusing on analyzing the wider spectrum of light over just the typically analyzed RGB wavelengths. Hence, it involves breaking down each pixel into various spectral bands and provide more extensive data through the captured image. While it has previously been majorly used in the military sector, with the growing availability of hyper-spectral data it has found its way to agriculture although not as much in the Indian subcontinent. Thus, by combining the concepts of precision agriculture and hyper-spectral imaging, a new level of analysis for soil fertility may be approached. With optimized analysis it has immense potential in the Indian subcontinent to aid in implementing modern farming techniques to maximize yields and profits for farmers [2].

With the advent of technological advances in various sectors, it can be crucial to maintain the relevant standards of modernity in fields such as agriculture particularly in the Indian subcontinent due to the prevalence of the same. One of the primary problems faced by farmers can be efficiently analyzing large fields and lands for type of soil and fertility of the soil in order to decide on various factors such as the purchase of fertilizers, types of crops that may be planted, and increasing productivity from potentially fertile lands [3, 4]. Specifically, for larger farms this can be a challenge due to the diverse soil types and landscapes present in the Indian subcontinent and require technology to help overcome the same. Hence, there is a need for a comprehensive and accurate technological tool to help optimize and maximize both crop yields and profits for farmers.

*School of Computer Science and Engineering, Vellore Institute of Technology, Vellore, India (lavanya.k@vit.ac.in).

2. Key Concepts.

2.1. Hyperspectral Imaging. Hyperspectral images are those in which each pixel is measured in one continuous spectrum. The spectral resolution is depicted in wave-numbers or nanometers. Spectral resolution can be defined as the interval between the different wavelengths that are measured in a specific range of wavelengths. The more the bands (spectral channels) the higher the spectral resolution. Hyperspectral Imaging is a technique that analyzes a wide spectrum of light, instead of just assigning colors like red, green or blue to each pixel [5].

2.2. Spectral Unmixing. Spectral Unmixing is a technique that has been used to analyze the mixture of components in remotely-sensed images for over 25 years. The most widely used method employs the use of a single set of endmembers (3-4) on the entirety of the image and then using a constrained least squares method to perform a linear unmixing. However, the variety of spectral unmixing techniques continues to grow, with most techniques being specific for its field of application.

2.3. NFINDR Algorithm. NFINDR algorithm is a technique that has its basis on the fact that in X spectral dimensions, the X-dimensional volume that is formed by a simplex (generalized notion of a triangle) with its vertices specified by the purest pixels, will always be larger than those formed by any other combination of pixels [6].

2.4. Cosine Similarity. Cosine similarity is a metric that is often used to determine the similarity between two particular objects (typically documents or samples). From a mathematical viewpoint, it looks to measure the cosine of the angle that exists between two vectors that are projected in a multidimensional space. Larger the angle, lesser the similarity.

2.5. pH Index. pH Index refers to the acidity or basicity of the soil sample in the hyperspectral image. It was a measure developed specifically for image processing in agriculture using the RGB values of each pixel present in the image. Different ranges of pH indexes indicate different ranges of pH, normally ranging from 5.58 to 7.50 pH.

$$\text{similarity} = \cos(\theta) = \frac{A \cdot B}{\|A\| \|B\|} = \frac{\sum_{i=1}^n A_i B_i}{\sqrt{\sum_{i=1}^n A_i^2} \sqrt{\sum_{i=1}^n B_i^2}}$$

3. Data set description. With the continuously growing versatility in Indian farmlands, it became evident that attempting to create a data set by collecting physical soil samples and comparing their fertility with the results obtained from the proposed model based on hyperspectral images would prove to be difficult. Thus, we decided to create our own data set. We focused on initially producing images as a mixture of various soil components ensure a minimum of ten different nutrients at a time. This is a blind creation, wherein the bands used in creating the image aren't used further in the analysis process. These images are assembled together and left unclassified thus leaving a scope for unsupervised classification later.

The research conducted is based on two main objectives. The first is to create a data set by producing hyperspectral images as a mixture of various soil components. In order to achieve this, the initial phase of the research focused on understanding the breakdown of soil components, and the basic requirements required in order for a particular sample of soil to be determined/classified as fertile or unfertile. The soil components, their determining features, their natural forms and other important characteristics were obtained from the USGS Hyperspectral Library and the results of these research were tabulated extensively.

The second phase of research focused on determining various classification and segmentation techniques that could be used to classify a given hyperspectral image as fertile or unfertile. The development of models based on unsupervised classification was chosen for the ambit of this paper. The extent of their results, due comparisons drawn and other details are further elaborated upon in the next section of this paper.

4. Methodology.

4.1. Generation of Hyperspectral Images. The process flow is initiated with the creation of the hyperspectral images. With the limitations faced due to the unavailability of large public datasets of hyperspectral images (HSI), there arose a necessity to manually produce a hyperspectral image dataset, which can ideally

simulate the required satellite images. With traditional HSI rarely procured in a pure form, and in order to accurately simulate the satellite images, external noise was factored during the production of the images for the dataset as well [7].

Beginning with MATLAB as the software of choice, a feature was employed that uses Gaussian fields to produce hyperspectral images. The bands that are wished to be included as a part of the image are inputted, and the function creates it as a Gaussian Random Field. Noise is then added to the Gaussian random distribution to mimic the disturbances that exist in remotely sensed satellite based hyperspectral images.

4.2. Spectral Unmixing using NFINDR Algorithm. Once these images are produced, the subsequent dataset created imitates one that would have been otherwise physically accumulated. The next stage involved includes the execution of spectral unmixing by employing the NFINDR algorithm. Spectral unmixing is carried out to breakdown a spectrum of mixed pixels into a set of its constituent spectra (also known as endmembers), along with a corresponding set of abundances (fractions that indicate the proportion of endmembers).

The NFINDR algorithm is basically an automated technique that is used to find the purest pixels present in an image. The main objective of this algorithm is to duplicate the successful technique (non-automated) of pinpointing the extreme points of an n dimensional scatter plot. The convex nature of existing hyperspectral data allows the NFINDR technique to be performed in relatively quick and straightforward method.

In the proposed process flow, an inbuilt function of MATLAB has been employed:

```
endmembers = nfindr (inputData, numEndmembers, Name, Value)
```

This function extracts the endmember signatures from hyperspectral data, by using the NFINDR algorithm. numEndmembers represents the number of endmember signatures that are to be extracted using the NFINDR algorithm. This syntax is used when the options for the number of iterations along with dimensionality reduction is required. The endmembers obtained have certain wavelengths that corresponds to specific components of soil. These endmembers can thus be used to classify different sections of soil in the hyperspectral image as fertile or unfertile [8].

4.3. NFINDR Algorithm.

1. Compute principal component bands and reduce spectral dimensionality of input data. Set number of PC bands to be extracted equal to number of endmembers to be extracted.
2. Randomly choose n number of pixel spectra from the reduced data as an initial set of endmembers.
3. Begin iteration 1, denote initial set of endmembers as compute volume using

$$V(E^{(1)}) = |\det(E^{(1)})|$$

where

$$E^{(1)} = \begin{bmatrix} 1 & 1 & \cdots & 1 \\ e_1^{(1)} & e_2^{(1)} & \cdots & e_p^{(1)} \end{bmatrix}$$

4. For the second iteration, select a new pixel spectra r , such that: $r \notin \{e_1^{(1)}, e_2^{(1)}, \dots, e_p^{(1)}\}$
5. Replace each endmember in the set with r and then compute the volume of the resulting simplex $V(E(2))$.
6. Replace the i th endmember in the set with r , and if the computed volume $V(E(2))$ is greater than $V(E(1))$. Thus arises an updated set of endmembers.
7. For each following iteration, select a new pixel spectra r and repeat the 5th and 6th step. The iterations end when the total number of iterations has reached the specified value.

4.4. Cosine Similarity based Accuracy prediction. Once the results of the spectral unmixing have been obtained, they become the second vector that will be used when determining the cosine similarity. The first vector used will be the plot of the band values that were originally used to create the hyperspectral images. Cosine similarity is used in order to determine the accuracy of the spectral unmixing and to identify if the endmember wavelengths obtained can be matched up to the wavelengths used in the production of the hyperspectral images in the first place.

4.5. Unsupervised Classification as Fertile/Infertile. In order to classify a particular hyperspectral image of a soil sample as fertile or infertile, numerous classification and segmentation algorithms were employed. The results drawn from these algorithms were compared, and subsequently K-Means Clustering and Agglomerative Clustering amongst the clustering techniques were found to display the best results while the neural network algorithms of ENet and DeeplavV3 provided highest reliability for classification, and FMM and Felzenszwalb algorithms provided the best results for pH index [9, 10].

4.5.1. K-Means Clustering. The objective of K-Means takes similar data points, and are grouped together to find subsequent underlying patterns. These collections of similar data points are referred to as a cluster.

A target number 'k' is defined, which indicates the number of centroids (real or imaginary location that represents the center of the cluster) that are needed in the dataset. Every data point is then assigned to each of the clusters by reducing the sum-of-squares (i.e. the algorithm identifies k number of centroid and then goes on to assign every data point to its nearest cluster, while ensuring to keep the centroids as small as accurately possible). During this process, each point refers to the results obtained from the NFINDR spectral unmixing process i.e. the spectral band values of a particular component of the original hyper spectral image. Using clustering with two centroids, the algorithm aims to separate the spectral bands as fertile or infertile, unsupervised.

The classification of the bands as fertile or infertile is then conducted by analyzing the centroid values, with the assumption that higher band values correspond to more fertile compounds, an assumption derived by analyzing the band values of various soil components. The fertility can hence be quantified based on comparing the aggregate presence of fertile components to the overall image while accuracy can be measured by comparing band values to their closest recognized material and the subsequent classification of such materials as fertile or infertile.

4.5.2. Fuzzy C-Means Clustering. The identity of each piece of data that corresponds to every center pixel is assigned by this technique proportion to the distance between the data point and the cluster center. The closer the data is from the cluster centre, the higher its cluster affinity. As a result, the sum of each data point must equal one, and the membership and cluster center's should be revised after each iteration. The advantages of this algorithm is that it gives the best result of overlapped data sets and as opposed to k-means clustering, where each data point should be exclusive to a single cluster center, membership here is allotted to each cluster center, so the data point can belong to more than one center [11].

$$\mu_{ij} = 1 / \sum_{k=1}^c (d_{ij}/d_{ik})^{(2/m-1)}$$

$$v_j = \left(\sum_{i=1}^n (\mu_{ij})^m x_i \right) / \left(\sum_{i=1}^n (\mu_{ij})^m \right), \quad \forall j = 1, 2, \dots, c$$

where n refers to the number of overall data points, v_j refers to the center of the j th cluster, m refers to the fuzziness index, c is the overall number of cluster centers, μ_{ij} is the affinity of the i th data point to the j th cluster center, d_{ij} is the distance between the i th data point and the j th cluster center.

The advantages of this algorithm is that it gives the best result of overlapped data sets and as opposed to k-means clustering, where each data point should be exclusive to a single cluster centre, membership here is allotted to each cluster center, so the data point can belong to more than one centre.

4.5.3. Agglomerative Clustering. Agglomerative clustering is essentially a strategy that is based on the concept of hierarchical clustering which is a type of cluster analysis that seeks to build a hierarchy of clusters. It relies on the core idea that objects are more related to nearby objects than objects which are further away.

Agglomerative clustering in specific is a bottom up approach where each observation starts in its own cluster, and pairs of clusters get merged as one moves up the particular hierarchy. The algorithm basically nests data points by building them from the bottom up, i.e. each data point acts as its own cluster and then they are combined together to create larger clusters.

Each data point refers to the spectral band values of a particular component obtained by executing spectral unmixing on the original hyper spectral image. By nesting these points from the bottom up, the algorithm uses unsupervised learning and aims to separate the spectral bands as either fertile or infertile,

The classification of the bands as fertile or infertile is then conducted by analyzing the resultant dendrogram, while working on the consistent assumption that cluster with the higher band values correspond to more fertile compounds. Thus the fertility can be quantified by comparing the aggregate presence of fertile components to the overall image and accuracy can be measured by comparing band values to their closest recognized material and the subsequent classification of such materials as fertile or infertile [12].

4.6. Segmentation Algorithms.

4.6.1. Fast Marching Method. It is a numerical technique that was developed in early 1996 to solve the boundary value problems that arose in the Eikonal equation. The algorithm works just like Dijkstra's algorithm but differs by how the node values are calculated. In the latter, a node's value is calculated by using a single neighboring node, whereas while solving the partial differential equation here, between 1 and n neighboring nodes are used.

During this process, the original noisy hyperspectral image is used as the input, while the algorithm aims to segment the image based on recognizable demarcations, boundaries and areas with familiar patterns. These familiarities are dependent on the FMM algorithm which creates two regions resulting in segments similar to that of the clustering results whenever possible. In cases of three or more segments, further grouping is conducted between the two largest regions and analysis is performed using these regions.

4.7. Algorithm Fast Marching Method.

1. Assume that the domain has been discretized into a mesh. Each node x_i has a corresponding value $U_i = U(x_i) \approx u(x_i)$.
2. Label the nodes as far (those which have not yet been visited), considered (those visited and value tentatively assigned) and accepted (those who have been visited and have been assigned a value permanently)
 - (a) Assign every node x_i , the value $U_i = +\infty$ and label them as far, and for all nodes $x_i \in \Omega$, set $U_i=0$ and label it x_i as accepted.
 - (b) For every far node, use the Eikonal update formula and calculate a new value for U' where $U' < U$ and then set $U_i = U'$. Label x_i as considered.
 - (c) Allow x' to be the considered node with the small U value. Label x' as accepted.
 - (d) Next, for every neighbor x_i of x' that isn't accepted, calculate a tentative U' .
 - (e) If $U' < U$ then $U_i=U'$. Change label to considered if it is labelled as far.
 - (f) If a considered node still exists, return to step (c), else terminate.

4.7.1. Efficient Neural Network. Efficient Neural Network (ENet) offers the capability to carry out real-time, pixel-by-pixel semantic segmentation. The method about 18 times faster, has 79 times less parameters, requires 75x less FLOPs and provides better accuracy to existing models.

The model architecture comprises of a 512 * 512 input image resolution. It can be broken down into the following steps:

- (i.) Feature Map Resolution: Limited down sampling has been carried out which has a main pro. Filters that operate on such down sampled images tend to possess a larger receptive field, which permits them to procure more contexts. Such a feature can be crucial when trying to separate between various classes.
- (ii.) Early down sampling: An important aspect for attaining great real-time functioning and performance is understanding that the cost of operating on bigger input frames can be costly. The ENet's first two blocks largely diminish the size of the input, and utilise only a tiny feature-maps set. Since visual information can be extremely spatially redundant, it can be abridged into a much more methodical representation.
- (iii.) Factorizing filters: A succession of processes that are utilized as part of the bottleneck module may also be visualized as breaking up a sizeable convolutional layer into a set of much more uncomplicated operations. This factorization permits greater speedups, and decreases redundancy by heavily reducing the number of parameters.

Name	Type	Output size
initial		$16 \times 256 \times 256$
bottleneck1.0	downsampling	$64 \times 128 \times 128$
$4 \times$ bottleneck1.x		$64 \times 128 \times 128$
bottleneck2.0	downsampling	$128 \times 64 \times 64$
bottleneck2.1		$128 \times 64 \times 64$
bottleneck2.2	dilated 2	$128 \times 64 \times 64$
bottleneck2.3	asymmetric 5	$128 \times 64 \times 64$
bottleneck2.4	dilated 4	$128 \times 64 \times 64$
bottleneck2.5		$128 \times 64 \times 64$
bottleneck2.6	dilated 8	$128 \times 64 \times 64$
bottleneck2.7	asymmetric 5	$128 \times 64 \times 64$
bottleneck2.8	dilated 16	$128 \times 64 \times 64$
<i>Repeat section 2, without bottleneck2.0</i>		
bottleneck4.0	upsampling	$64 \times 128 \times 128$
bottleneck4.1		$64 \times 128 \times 128$
bottleneck4.2		$64 \times 128 \times 128$
bottleneck5.0	upsampling	$16 \times 256 \times 256$
bottleneck5.1		$16 \times 256 \times 256$
fullconv		$C \times 512 \times 512$

Fig. 4.1: ENET network architecture

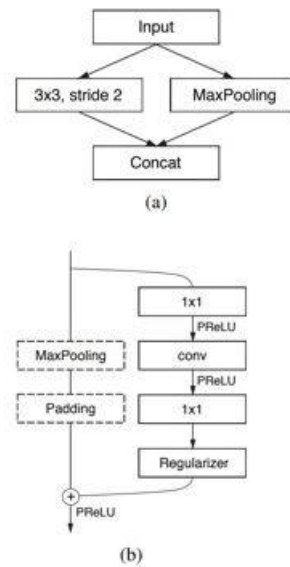


Fig. 4.2: (a) Graphical representation of the first block (b) Bottlenecks

(iv.) Regularization: While the concept of stochastic depth was attempted, in order to increase accuracy, it became apparent that dropping entire branches is actually a special case of applying Spatial Dropout. In this process either all of the channels, or none of them are ignored, and this spatial dropout is placed upon completion of the convolutional branches, just before the inclusion, which came out to work more efficiently compared to the traditional stochastic depth.

As visible in the network architecture, each bottleneck module is made up of the multiple components

which are detailed as follows:

- A 1x1 projection that minimises the number of dimensions.
- A main convolution layer (conv) (full, dilated, or regular convolution) (3x3).
- Expansion 1x1.
- PReLU and Batch Normalization are placed between all convolutional layers.
- Next, a max pooling layer is added to the main branch if down-sampling is the bottleneck. A 2x2 convolution with stride=2 is also used in place of the first 1x1 projection. This is followed by zero padding the activations to match the amount of feature maps, and occasionally using asymmetric (5 * 1 and 1 * convolutions).

The system architecture is composed of five stages. Stages 1, 2, and 3 (the encoder) each have five bottleneck blocks (with the exception of Stage 3 which does not down-sample). Stages 4, and 5 constitute the decoder and possess three and two bottlenecks respectively.

The last step is a fullconv, which produces a final output with the dimensions $C * 512 * 512$, where C is the number of filters.

4.7.2. Felzenszwalb Segmentation. An important concept to note before delving into the Felzenszwalb Segmentation is the Minimum Spanning Tree (MST) which refers to a cycle-free, graph's edges' minimum-weight subset which connects every node.

Felzenszwalb published an image segmentation approach platformed on Kruskal's MST algorithm in 2004 where analysis of edges is performed in sequence of increasing weightage, and the pixels of the endpoints are combined into a section if they do not generate a cycle in the graph and are 'similar' to the pixels of existing regions. Utilising the disjoint-set data structure, it can be possible to detect cycles in near-constant time. A comparison between the weight and a per-segment threshold is performed by heuristics in order to determine pixel similarity. The technique generates a forest of disjoint MSTs, each of which corresponds to a segment. As sorting edges in linear time is attainable using counting sort, the algorithm's complexity is quasi-linear.

Utilising a rapid, MST-based clustering on the image grid, this approach provides an over-segmentation of a multichannel (i.e. RGB) image. The parameter 'scale' is then used to determine the level of observation with less and larger parts generally being associated to a greater scale. Next, the diameter of a Gaussian kernel 'sigma', is used to smooth the image before segmentation. The only way to control the quantity of created segments as well as their size is by using the scale and the size of individual segments within a picture might vary dramatically depending on the local contrast. Similarly, the euclidean distance between pixels in colour space is used by the algorithm for RGB images.

For the analysis of soil, the coloured version of the hyperspectral is used as the input image with x scale resulting in 90-100 segments. While most of the resultant segments are of sizes less than 500 pixels, the larger segments can be utilised to analyse fertility of soil. The major drawback of this method is the over-segmentation of the image which in turn creates a bottleneck during result analysis.

4.7.3. Deeplabv3 with Pascal VOC model. One of the difficulties in utilising deep convolutional neural networks (DCNNs) to segment objects in images is that as the input feature map shrinks, the network traverses as a consequence of which, information about objects of a smaller scale can be lost.

DeepLab's contribution is the use of atrous convolutions, or dilated convolutions, to retrieve denser features with greater preservation of information from objects of a different scale [2–3]. The atrous rate is a parameter in atrous convolutions that correlates to the stride at which the input signal is sampled. It's the same as putting 'r-1' zeros between two successive filter values along each spacial dimension in figure 4.2. Because 'r=2' in this situation, the number of zeros between each filter value is 1. The goal of this technology is to be able to change the filter's field-of-view and how dense the features are computed simply by altering r rather than learning additional parameters. The output stride, which is the ratio of the input picture resolution to the output image resolution, is tweaked.

DeepLabv3 adds an image-level functionality to the ASPP module, allowing it to capture longer-range data. It also has batch normalisation options to make training easier and uses atrous convolution to extract output features at different output strides during training and evaluation, allowing BN to be trained at output stride = 16 and evaluated at output stride = 8, resulting in great performance at output stride = 8.

Table 5.1: Spectral Unmixing Results.

Image	Image 1	Image 2	Image 3	Image 4	Image 5
Percentage Error	2.1112%	2.6917%	2.3810%	2.6557%	2.1118%
Identified Soil Components	alunite_cu91-217h.23978.asc	alun_na_mv00-11a.23894.asc	acid_mine_drain_assem2.23799.asc	alunite_cu91-217h.23978.asc	alunite_cu91-217h.23978.asc
	alunite_mix_mv2-ar3.25474.asc	alunite_cu91-217h.23978.asc	alunite_cu91-217g1.23924.asc	alunite_cu98-5c.24129.asc	alunite_nh4-jar_nmnh145596.24230.asc
	alunite_na_dickite_mv99-6-26b.23945.asc	alunite_cu98-5c.24129.asc	alunite_cu91-217h.23978.asc	alunite_mix_mv2-ar3.25474.asc	calcite_talc_pc99-1g.24536.asc
	beidellite_montmor_gds124.24340.asc	alunite_mix_mv2-ar3.25474.asc	alunite_na_dickite_mv99-6-26b.23945.asc	alunite_nh4-jar_nmnh145596.24230.asc	constructed_mixtures_calc_epid.24594.asc
	calcite_talc_pc99-1g.24536.asc	alunite_nh4-jar_nmnh145596.24230.asc	beidellite_montmor_gds124.24340.asc	calcite_talc_pc99-1g.24536.asc	constructed_mixtures_chi_epid.24789.asc
	constructed_mixtures_calc_epid.24573.asc	constructed_mixtures_chi_epid.24766.asc	constructed_mixtures_calc_epid.24594.asc	constructed_mixtures_chlor_calc.24833.asc	constructed_mixtures_chlor_calc.24833.asc
	constructed_mixtures_calc_epid.24594.asc	constructed_mixtures_chlor_calc.24833.asc	constructed_mixtures_chlor_epid.24833.asc	constructed_mixtures_chi_epid.24870.asc	illite-high-ai_cu00-5b.25438.asc
	constructed_mixtures_chi_epid.24811.asc	dolo_calc_talc_pc99-1a.25017.asc	goethite_phylite_cu91_236a.25213.asc	goethite_phylite_cu91_236a.25213.asc	kaolinite_wal+other_cu00-19a.25536.asc
	goethite_phylite_cu91_236a.25213.asc	goethite_phylite_cu91_236a.25213.asc	halloysite_cu91-242d.25302.asc	hydrate_volcanic_glass_cu01-4a.25417.asc	kaolinite_wal+other_cu91-200a.25557.asc
	hematite_tuff_cu91_223.25396.asc	gyp_jar_ill_brom1.25237.asc	hematite_tuff_cu91_223.25396.asc	muscovite-medhi-AI_CU91-252d.26143.asc	muscovite-medlow-AI_cu91-250a.26166.asc
	kaolinite_wal+other_cu00-19a.25536.asc	hydrate_volcanic_glass_cu01-4a.25417.asc	illite-high-ai_cu00-5b.25438.asc	muscovite-medlow-AI_cu91-250a.26166.asc	nontronite_cu00-13a.26189.asc
	musc_pyro_pyrp1.26100.asc	illite-high-ai_cu00-5b.25438.asc	limestone_cu02-11a.25827.asc	pyro_musc_pyrp1.26313.asc	opal_cu00-15e.26266.asc
	nontronite_cu00-13a.26189.asc	limestone_cu02-11a.25827.asc	muscovite-medhi-AI_CU91-252d.26143.asc	pyroxene_basalt_cu01_20a.26360.asc	stonewall_playa.26390.asc
	opal_cu00-15e.26266.asc	muscovite-lowAI_cu98-8h.26121.asc	stonewall_playa.26390.asc	talc_clinochi_hc327.26428.asc	
	pyro_musc_pyrp1.26313.asc				
	stonewall_playa.26390.asc				
	talc_clinochi_hc327.26428.asc				

Table 5.2: Unsupervised Clustering Results.

Image	Clustering Algorithms						Actual Result
	K-Means Result	Percentage Fertility	Agglomerative Result	Percentage Fertility	Fuzzy C-Means Result	Percentage Fertility	
Image 1	Infertile	25%	Fertile	65%	Infertile	45%	Infertile
Image 2	Infertile	40%	Infertile	5%	Infertile	40%	Infertile
Image 3	Infertile	45%	Infertile		25%	Fertile	55%
Image 4	Infertile	40%	Infertile		10%	Infertile	45%
Image 5	Fertile	85%	Fertile		90%	Fertile	55%

The implementation in the current scenario uses the “PASCAL VOC” dataset which is a popular dataset of choice while building models that are being conditioned for image classification and segmentation.

5. Results and Discussions. Using the above-mentioned method, the considered area in each year from 2020 to 2022 is classified into fertile/unfertile sectors. The parameters that are mentioned below are: Class: Each class identifies the global constant based on which the classification is done.

Fertility Percentage %: The percentage shows the percentage covered by the class compared to the other Classes.

Epochs: The number of iterations for which the image is processed to reduce error percentage

5.1. Spectral Unmixing. Using the NFINDR Spectral Unmixing algorithm in order to identify the component endmembers of a hyperspectral image, the results obtained were as in Table 5.1. The two properties obtained as results were the individual soil components present in the soil hyperspectral image (refer to table) and the percentage similarity to the endmembers making up the original image measured using cosine similarity.

As per the obtained results (Table 5.1), the NFINDR technique presents itself as a highly accurate and efficient method of spectral unmixing for the precision agriculture use case. With similarity values consistently lower than five percent, the endmembers obtained can be adequately identified as specific soil components through comparison of wavelength values. The results present an opportunity for the use of hyperspectral imaging and spectral imaging in the field of agriculture to accurately capture soil components over large areas with little physical overhead, a problem currently found in the sector. Additionally, decisions regarding fertility, regions of improvement, potential crop yields etc. can be taken with technological evidence [15].

5.2. Unsupervised Clustering. Unsupervised clustering algorithms were used for classifying component soil endmembers based on their fertility utilizing the results of the spectral unmixing. The algorithms used were K-Means Clustering, Agglomerative Clustering and Fuzzy C-Means Clustering. The results obtained were as in Table 5.2.

The properties obtained for each algorithm were the classification result i.e. whether the soil sample was adjudged to be majorly fertile or infertile, and the percentage fertility measured based on the size of the cluster and percentage presence of fertile or infertile components in the soil sample image (Table 5.2). The actual result was obtained using a combination of subjective analysis of the obtained soil endmembers and the pH index of the soil image as a whole.

Table 6.1: Segmentation results based on fertility

Image	Image Segmentation Algorithms												Actual Result	
	K-Means Segmentation Result	pH Value	FMM Segmentation Result	pH Value	Felzenszwalb Segmentation Result	pH Value	DeepLabV3 Result	pH Value	ENET Result	pH Value	Result	pH Value	Result	pH Value
Image 1	Infertile	0.0259	Infertile	0.0355	Infertile	0.0395	Infertile	0.0273	Infertile	0.0603	Infertile	0.0117		
Image 2	Infertile	0.0329	Infertile	0.0458	Infertile	0.0405	Infertile	0.0563	Infertile	0.0544	Infertile	0.0123		
Image 3	Fertile	0.0308	Infertile	0.0322	Infertile	0.0403	Infertile	0.0308	Infertile	0.0624	Infertile	0.0098		
Image 4	Infertile	0.0366	Infertile	0.0238	Infertile	0.0384	Infertile	0.0405	Infertile	0.0589	Infertile	0.0150		
Image 5	Fertile	0.0409	Fertile	0.0507	Fertile	0.0419	Fertile	0.0304	Fertile	0.0398	Fertile	0.0221		

6. Results and Discussions. The results provide crucial insight into the potential of clustering algorithms in the field of precision agriculture. Unsupervised clustering algorithms provide reasonable accuracy with respect to fertility classification and further insight through the fertility percentage measure. Apart from highlighting the usefulness of hyperspectral imaging in precision agriculture by directly determining fertility, it indicates the potential for further field-based research in the sector hence creating a platform for supervised algorithms and increasing the use-case for hyperspectral imaging in precision agriculture. Further, due to the high similarity between original soil components and spectral unmixing results, the prerequisites for the utilization of clustering algorithms are easily satisfied and provide promising results. Another notable advantage of utilizing clustering algorithms is the low overhead required for analysis in comparison to image segmentation. Unlike the latter, clustering directly uses spectral endmembers which require less physical memory to store and processing power required is significantly lower due to the lower complexity and requirements. This is particularly consequential as in agricultural fields, lower hardware and software requirements are preferred with lack of accessibility, resources and connectivity being features of rural India.

In comparing the three algorithms, K-Means clustering and Agglomerative clustering techniques have the highest accuracy in fertility classification with the latter preferred due to the lack of dependence on initial centroid values and subjectivity created in using the former. While the Fuzzy C-Means is adequately accurate, the results of the other tested techniques offer better results.

6.1. Image Segmentation. Image segmentation algorithms were used for classifying regions of the soil sample image based on their fertility using the colorized hyperspectral image. The algorithms used were K-Means Segmentation, FMM Segmentation, Felzenszwalb Segmentation, DeeplabV3 and ENET segmentation.

The properties obtained for each algorithm were the classification result i.e. whether the largest segment obtained was adjudged to be fertile or infertile, and the pH index of the largest segment obtained post-segmentation. The former is measured comparing the pH index of the largest and the next-largest segment obtained from the segmentation process. pH index was measured through the RGB index values of each individual pixel of the image (add reference). The actual result was obtained using a combination of subjective analysis of the obtained soil endmembers and the pH index of the soil image as a whole.

As per the obtained results, image segmentation is yet another potential avenue in precision agriculture using hyperspectral imaging. Working on the principle of classifying regions of fertility based on the soil component endmembers, the major function of such segmentation is the identification of fertile soil in large plots of land. This in turn can help agriculturists predict crop yields and prioritise such identified regions for the same. Additionally, by classifying whole regions (as captured by the image) as fertile or infertile it can help states and agriculturists during the purchase and transfer of land as well as during harvest, to identify regions of high yield and prioritising such regions. The pH index measure provides further insight into the properties of the soil hence giving quantifiable data to work with. For selection of comparison algorithms, we have taken five random images. Results are shown in table 6.2. While in other Algorithms, the variation in results according to noise level is high. But in PSNR it is comparatively low. As shown in table 6.1 PSNR is a good option to use for finding fertility of selected area in 2020 and 2022.

PSNR demonstrates that the picture is of acceptable quality.

$$PSNR = \log_{10} \frac{MAX_k^2}{MSE} \quad (6.1)$$

For SSIM calculation, reference image C2 is a constant added to avoid instability when other terms are

Table 6.2: Performance error metrics comparison

Image	Epoch	Felzenszwalb	Deeplabv3	Enet
		MSE	PSNR	SSIM
1	100	87.86	31.51	0.94
2	100	65.51	29.96	0.89
3	100	45.04	28.77	0.85
4	100	67.93	29.80	0.88
5	100	89.33	31.44	0.93

close to zero. Correlation factor is calculated by Eq. (6.2)

$$s(x, y) = \frac{2\sigma_{xy} + C_2}{\sigma_x\sigma_y + C_2} \quad (6.2)$$

where σ_{xy} in Eq. (6.2) is a covariance between the two images and C3 for avoiding instability. Finally, combining all the factors equations, namely Eq. (6.1), Eq. (6.2) we will get SSIM as shown in Eq. (6.3)

$$SSIM(x, y) = \frac{(2u_xu_y + C_1)(1\sigma_x + \sigma_y + C_2)}{(\sigma_x^2 + \sigma_y^2 + C_2)(u_x^2 + u_y^2 + C_1)} \quad (6.3)$$

where σ_{xy} in Eq. (6.3) is a covariance between the two images and C3 for avoiding instability. It has indistinguishable units of estimation from the square of the amount being determined like variance, which is based on original data x, y , and is defined as in Eq. (6.3).

MSE is a full reference metric, and the qualities more like zero are better. The fluctuation of the estimator and its bias are both fused with the mean squared error.

$$MSE = \frac{1}{mn} \sum_{i=0}^{m-1} \sum_{j=0}^{n-1} [I(i, j) - K(i, j)]^2 \quad (6.4)$$

All algorithms tested, with the exception of the K-Means image segmentation, show high accuracy with respect to fertility classification while the more primitive methods of FMM and Felzenszwalb show higher accuracy for the pH index. However, the neural network algorithms of DeeplabV3 and ENET are preferred due to their higher reliability as seen through the higher difference between pH index values of each segmented region.

The drawback however stems from the problem of overhead where the latter algorithms require high computing power and prerequisite software in order to function, an issue overcome by using the former techniques. On the whole, image segmentation requires higher overhead for usage as the input is raw hyperspectral images which take up more storage and require higher software and hardware to run and maintain.

7. Conclusion. In general, the application of hyperspectral imaging in precision agriculture is a potentially lucrative research subject with significant application in the rural Indian areas. The solution's scope includes both short-term and long-term considerations. The former includes immediate analysis of soil fertility in fields, estimation of crop yields, maximization of profits, and uses in land transfer. The latter includes quantification of fertility using imaging rather than manual testing, analysis of the long-term fertility of land, and the effectiveness of various agricultural practices, among other things. When compared to the manual laboratory setting for testing soil, the results' high accuracy establishes the conditions for a contemporary, trustworthy data source for agriculture experts and farmers alike with fewer overhead and expenses.

Hyperspectral imaging is a prospective addition to the same, especially with the expansion of digital technology in rural areas and the introduction of technology. The findings and subsequent analysis also aid

in filling a research gap in the application of unsupervised classification models in the field as well as the dependability of produced hyperspectral image datasets. The latter is particularly important because it is less difficult, costs less to operate, and uses fewer digital resources than developing, testing, and deploying supervised algorithms. Even in the case of supervised algorithms, the numerous properties and features that can be derived from digitally made hyperspectral pictures serve as a foundation for training and testing such algorithms without the need for manual analysis and expensive research costs.

REFERENCES

- [1] L. LIU, M. JI, AND M. BUCHROITHNER *Transfer learning for soil spectroscopy based on convolutional neural networks and its application in soil clay content mapping using hyperspectral imagery* Sensors, vol. 18, no. 9, Sep. 2018, Art. no. 3169.
- [2] A. K. PATEL, J. K. GHOSH, S. PANDE AND S. U. SAYYAD *Deep-Learning-Based Approach for Estimation of Fractional Abundance of Nitrogen in Soil From Hyperspectral Data* in IEEE Journal of Selected Topics in Applied Earth Observations and Remote Sensing, vol. 13, pp. 6495-6511, 2020, doi: 10.1109/JSTARS.2020.3039844.
- [3] LI, HONGYANG, SHENGYAO JIA, AND ZICHUN LE *Quantitative Analysis of Soil Total Nitrogen Using Hyperspectral Imaging Technology with Extreme Learning Machine*. Sensors (Basel, Switzerland) vol. 19,20 4355. 9 Oct. 2019, doi:10.3390/s19204355
- [4] CHEN, YUN, YUQIANG LI, XUYANG WANG, JINLIANG WANG, XIANGWEN GONG, YAYI NIU, AND JING LIU. *Estimating soil organic carbon density in Northern China's agro-pastoral ecotone using vis-NIR spectroscopy* Journal of Soils and Sediments. 2020, 20(10):3698-711.
- [5] ANNA CHLINGARYAN, SALAH SUKKARIEH, BRETT WHELAN *Machine learning approaches for crop yield prediction and nitrogen status estimation in precision agriculture: A review* Computers and Electronics in Agriculture, Volume 151, Pages 61-69, ISSN 0168- 1699,2018, doi: 10.1016/j.compag.2018.05.012.
- [6] L. Sun, F. Wu, T. Zhan, W. Liu, J. Wang and B. Jeon *Weighted Nonlocal Low-Rank Tensor Decomposition Method for Sparse Unmixing of Hyperspectral Images* in IEEE Journal of Selected Topics in Applied Earth Observations and Remote Sensing, vol. 13, pp. 1174-1188, 2020, doi: 10.1109/JSTARS.2020.2980576.
- [7] SOMENATH BERA AND VIMAL K. SHRIVASTAVA *Analysis of various optimizers on deep convolutional neural network model in the application of hyperspectral remote sensing image classification* International Journal of Remote Sensing, 41:7, 2664-2683, 2019, doi: 10.1080/01431161.2019.1694725
- [8] CHANG LI, YU LIU, JUAN CHENG, RENCHENG SONG, JIAYI MA, CHENHONG SUI, XUN CHEN *Sparse unmixing of hyperspectral data with bandwise model*, Information Sciences Information sciences, 512, pp.1424-1441,2020.
- [9] YUAN, YUAN, ZIHAN ZHANG, AND QI WANG *Improved Collaborative Non- Negative Matrix Factorization and Total Variation for Hyperspectral Unmixing* IEEE Journal of Selected Topics in Applied Earth Observations and Remote Sensing. PP. 1-1,2020
- [10] SONG, Y.-Q.; ZHAO, X.; SU, H.-Y.; LI, B.; HU, Y.-M.; CUI, X.-S. *Predicting Spatial Variations in Soil Nutrients with Hyperspectral Remote Sensing at Regional Scale*. Sensors , 18,2018, doi: 10.3390/s18093086
- [11] Haijun Qi, Tarin Paz-Kagan, Arnon Karnieli, Xiu Jin, Shaowen Li, Evaluating calibration methods for predicting soil available nutrients using hyperspectral VNIR data, Soil and Tillage Research, Volume 175, Pages 267-275, ISSN 0167 1987,2018
- [12] JIA S, LI H, WANG Y, TONG R, LI Q. *Hyperspectral Imaging Analysis for the Classification of Soil Types and the Determination of Soil Total Nitrogen*. Sensors (Basel),(10),2017, doi:10.3390/s17102252
- [13] LIGUO WANG, SAN WANG, XIUPING JIA AND TIANYI BI *A Novel Hyperspectral Unmixing Method based on Least Squares Twin Support Vector Machines*, European Journal of Remote Sensing, 54:1, 72-85, DOI: 10.1080/22797254.2021.1877572
- [14] PENG Y, ZHAO L, HU Y, WANG G, WANG L, LIU Z. *Prediction of Soil Nutrient Contents Using Visible and Near-Infrared Reflectance Spectroscopy*. ISPRS International Journal of Geo-Information, 8(10):437,2019, doi: 10.3390/ijgi8100437
- [15] XUE SONG, YONGXIANG GAO, ZHIGUANG LIU, MIN ZHANG, YONGSHAN WAN, XINYANG YU, WENLONG LIU AND LEI LI *Development of a predictive tool for rapid assessment of soil total nitrogen in wheat-corn double cropping system with hyperspectral data*, Environmental Pollutants and Bioavailability, 31:1, 272-281,2019, DOI: 10.1080/26395940.2019.1679041

Edited by: Vinoth Kumar

Received: Jul 31, 2022

Accepted: Oct 19, 2022